ARTICLE

An Abrasion Resistant TPU/SH-SiO$_2$ Superhydrophobic Coating for Anti-Icing and Anti-Corrosion Applications

Jiakun Shi[1], Bizhu Zhang[1], Xin Zhou[1], Runxian Liu[1], Jun Hu[1,2,*], Huaan Zheng[1] and Zhong Chen[3,*]

[1]School of Chemical Engineering, Northwest University, Xi'an, 710069, China

[2]School of Chemical Engineering, Xi'an Key Laboratory of Special Energy Materials, Northwest University, Xi'an, 710069, China

[3]School of Materials Science and Engineering, Nanyang Technological University, 639798, Singapore

*Corresponding Authors: Jun Hu. Email: hujun32456@163.com; Zhong Chen. Email: ASZChen@ntu.edu.sg

ABSTRACT

As a passive anti-icing strategy, properly designed superhydrophobic coatings can demonstrate outstanding performances. However, common preparation strategies for superhydrophobic coatings often lead to environmental pollution, high energy-consumption, high-cost and other undesirable issues. Besides, the durability of superhydrophobic coating also plagues its commercial application. In this paper, we introduced a facile and environment-friendly technique for fabricating abrasion-resistant superhydrophobic surfaces using thermoplastic polyurethane (TPU) and modified SiO$_2$ particles (SH-SiO$_2$). Both materials are non-toxicity, low-cost, and commercial available. Our methodology has the following advantages: use of minimal amounts of formulation, take the most streamlined technical route, and no waste material. These advantages make it attractive for industrial applications, and its usage sustainability can be promised. In this study, the mechanical stability of the superhydrophobic surface was evaluated by linear wear test. It is found that the excellent wear resistance of the superhydrophobic coating benefits from the characteristics of raw materials, the preparation strategy, and the special structure. In anti-icing properties test, the TPU/SH-SiO$_2$ coating exhibits the repellency to the cold droplets and the ability to extend the freezing time. The electrochemical corrosion measurement shows that the as-prepared superhydrophobic surface has excellent corrosion resistance that can provide effective protection for the bare Q235 substrates. These results indicate that the TPU/SH-SiO$_2$ coating possesses good abrasion resistance and has great potential in anti-corrosion and anti-icing applications.

KEYWORDS

Coating; superhydrophobic; abrasion resistance; anti-icing; anti-corrosion

1 Introduction

Low-temperature methanol washing is a mature and common process for acid gas (CO$_2$, H$_2$S, COS, etc.) removal in industry. Due to the excellent solubility of methanol for acid gas at low temperatures, cold methanol is used as an absorption solvent to remove acid gas from the feed gas. However, under a low temperature and humid environment, water will turn into ice on the tube surface, while the corrosive media will induce corrosion of equipment. And then lead to pipeline corrosion failure, which causes the

leakage of the medium in the pipeline, resulting in waste of resources and environmental pollution, and even lead to huge economic losses and serious personal injury.

Superhydrophobic coating is an alternative or supplementary strategy for anti-icing applications [1–5]. Given the low adhesion of superhydrophobic coating to ice and the ability to delay the icing process, many researchers have extensively studied the icephobic performance of this passive anti-icing strategy [6–8]. Farhadi et al. [9] studied several superhydrophobic coatings with different morphologies and surface chemical compositions by spin coating or impregnation, and evaluated their ice resistance durability using a low-temperature wind tunnel. Yang et al. [10] prepared an aluminium-based coating with superhydrophobicity by etching followed by low energy surface modification. The prepared surface coating can delay the freezing time by 600–700 s. Shen et al. [11] compared the anti-icing ability of Ti_6Al_4V alloy before and after fluoroalkylsilane modification. They found that the modified surface has significantly prolonged the water freezing process, and the water droplet can rebound at sub-zero temperature.

Superhydrophobicity can be achieved onto various metal/non-metal materials surfaces [12–16]. For the metal substrates, which surfaces are hydrophilic, it is necessary to form a micro-nano rough structure on its surface and then modify it with low surface energy materials to obtain superhydrophobic properties. Unfortunately, the methods or raw materials used in obtaining the graded roughness often cause undesirable issues [17,18]. For instance, chemical etching methods require the corrosive procedure, while H_2SO_4, HCl, HNO_3, and NaOH solutions are often used [19,20], which have a negative effect on the environment to a certain extent. Wu et al. [21] used a femtosecond laser, whereas Sethi et al. [22] used carbon nanotube (CNT) to prepare superhydrophobic steel surfaces. Both professional equipment and expensive raw materials have led to an increase in manufacturing costs. Besides, the low-surface-energy chemicals and micro-nano rough structures can be easily damaged under some harsh application environments. Precipitation, sand dust and mechanical abrasion/wear may change the surface morphology and/or chemistry, leading to partial or complete loss of the superhydrophobic properties [23–27]. As a result, these challenges cannot meet the demand of large-scale industrial production and commercial applications.

This research aims to develop a simple and environment-friendly method for the preparation of durable superhydrophobic surfaces. A layer-by-layer forming process is applied to produce superhydrophobic coating, and the superhydrophobicity is realized by perfluorocarbon chain-containing compounds. This coating is composed of the thermoplastic polyurethane (TPU) layer at the bottom and the SiO_2 layer at the top. TPU is used as an adhesive that exhibits promising characteristics such as excellent elasticity, abrasion and weather resistance, and high strength. The surface roughness comes from the SiO_2 nanoparticles owing to high hardness, outstanding mechanical stability and easy structure adjustment. Both materials are non-toxic, low-cost, commercially and widely available. Since no special equipment and professional tools are required, the technical route has been simplified. The whole preparation process has no strict process parameters, all raw materials are effectively utilized, and no harmful substances are discharged. These advantages make it attractive for industrial applications, and its usage sustainability can be promised. We systematically investigated the wettability, mechanical stability, ice repellency and anti-corrosion performance of the superhydrophobic coating.

2 Experiment

2.1 Materials and Methods

In a typical process, Q235 steel with a thickness of 2 mm and a dimension of 2 cm × 3 cm was used as the metal substrate. The chemicals used were thermoplastic polyurethanes (TPU 95A, Bayer), N,N-dimethylformamideethanol (DMF), Trimethoxy(1H,1H,2H,2H-heptadecafluorodecyl)silane

($C_{13}H_{13}F_{17}O_3Si$, THFS), SiO_2 (15 ± 5 nm), and anhydrous ethanol (ETOH). All chemicals were analytically pure and can be used without further purification.

The TPU/SH-SiO$_2$ superhydrophobic coatings were made as follows:

Modification of SiO$_2$ nanoparticles by THFS. 4 g of SiO$_2$ nanoparticles were added into a mixture of 100 g of 1 wt% THFS-ETOH solution and under stirring for 30 min vigorously. The mixture was dried under vacuum at 100°C for 3 h after stirring. Then the solid was ground by mortar in order to collect the silica nanoparticles. These particles were named as SH-SiO$_2$ in this paper since the surface of the silica particles are covered with the hydrophobic groups and good water resistance.

Preparation of TPU basal layer. Before preparation, TPU was dissolved in DMF to make the 0.3 g/ml TPU/DMF film-forming solution, and the steel substrates were polished by abrasive paper and ultrasonically cleaned to remove rust and grease. Then, a small amount of film-forming solution (about 0.5–1.0 ml) was evenly coated on the substrate by a scraper and cured at 100°C for 5 min. To obtain desirable mechanical properties, this coating step should be repeated at least 3–5 times so that the TPU layer could reach the required thickness (More details can be found in Section 1 of Supplementary Information).

Fabrication of TPU/SH-SiO$_2$ superhydrophobic coating. As illustrated in Fig. 1a, a layer of uncured TPU/DMF solution on the TPU basal layer covered with 0.5 g SH-SiO$_2$, and a pressure of 7.5 kPa applied on top of the coating through a flat plate in order to embed the silica particles into the TPU layer. Removed the force after one minute, then put the sample into the vacuum at 100°C for 5 min. When the coating was cured completely, the excess particles were recycled, and a superhydrophobic film was formed.

2.2 Surface Analysis

The surface morphologies and chemical compositions of the substrates were characterized by field emission scanning electron microscopy (FESEM, ZEISS SIGMA 300, Germany) and X-ray photoelectron spectroscopy (XPS, Shimadzu-Kratos AXIS UltraDLD, Japan), respectively. The water contact angle (WCA) and sliding angle (SA) of the coatings were evaluated using a JinHe JY-PHb contact angle measurement device with 5 μL of water droplets. During the measurement, each sample was measured at five different locations and the average values were reported. The same method was used to measure the CA and SA of glycerin, and to characterize the influence of the solution pH value (adjusted by H_2SO_4 or NaOH addition) on WCAs and SAs of the coating.

2.3 Abrasion Test

In the abrasion resistance test, a piece of 80 Grit SiC sandpaper was placed on a floor before the superhydrophobic surface was laid on top with its coating side facing the sandpaper. Then different weights were uniformed applied to the coating substrate, leading to 2.5 kPa, 5.0 kPa, 10.0 kPa pressure on the test surface, respectively. Abrasion was carried out by sliding the coating with substrate slowly and uniformly along one direction for 0.5 m in a test cycle. The corresponding WCAs and SAs were measured after every cycle. Surface profiles were collected using a profiler optical (Brüker Veeo Contour GT-K1, America) and a digital microscope. The roughness (R_a) was calculated using the height data from the entire image.

2.4 Icing Experiments

The dynamic performance of the superhydrophobic coating at low temperatures was evaluated by recording the process of water droplets falling from 10 cm above the sample impacting the surface using a high-speed camera (Phantom LAB310, USA) at 3200 frames per second. In addition, icing delay performance was also recorded at –20°C. Bare substrate and the one with superhydrophobic coating were compared.
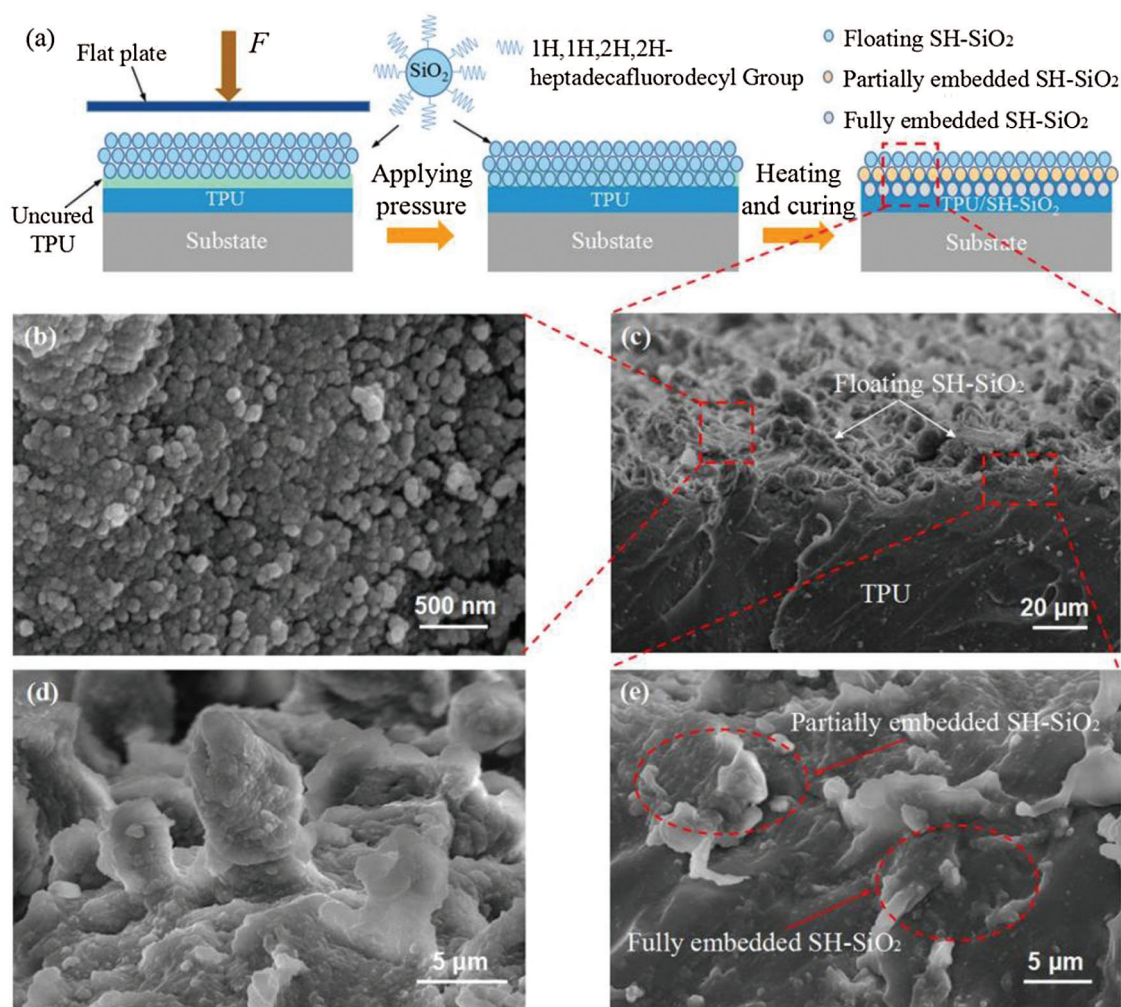
Figure 1: (a) Schematic diagram of the formation mechanism of the TPU/SH-SiO$_2$ coating with superhydrophobicity; High-resolution SEM images of the coating (b) surface and (d) papillary protrusions on it; (c) SEM image of the coating cross-section and (e) High-resolution SEM image of the coating cross-section

2.5 Electrochemical Measurement

The electrochemical corrosion measurement was performed with a three-electrode cell in an electrochemical workstation (CS350, Wuhan Corr Test Instrument Co., Ltd., China) under ambient condition. The saturated calomel electrode (SCE), Pt plate, and samples with an open area of 0.86 cm^2 were used as the reference, counter, and working electrode, respectively. Each electrochemical impedance spectroscopic (EIS) measurement was carried out in the frequency range of 10^{-2} to 10^5 Hz and started after the sample was immersed in 3.5 wt% NaCl aqueous or other corrosion solutions for 30 min. The immersion could ensure the accuracy of measurement data.

3 Results and Discussion

3.1 Surface Morphology, Chemical Compositions and Wettability

The SEM images of the TPU/SH-SiO$_2$ superhydrophobic coating surface and cross-section are shown in Figs. 1b–1e. It can be observed from the high-resolution SEM (Fig. 1b) that the aggregation of silica particles

leads to the appearance of nanoscale roughness. These SH-SiO$_2$ particles range in size from dozens of nanometers to several hundreds of nanometers. In Figs. 1c and 1d, the more intense aggregation of silica particles produce a large number of irregular papillae, resulting in obvious microscale roughness. The hierarchical micro-nano structures and low-surface-energy silica particles, thus leading to superhydrophobicity. Figs. 1c and 1e are the cross-section images of the coating. It could be divided into three types for the silica particles according to the relationship between its and TPU layer [28]. The partially embedded and fully embedded SH-SiO$_2$ indicate that the particles are embedded in the uncured TPU under the external force.

XPS measurements of the SH-SiO$_2$ were characterized to correlate the chemical composition of the TPU/SH-SiO$_2$ coating surface with its superhydrophobicity. Fig. 2 displays the XPS spectra of the superhydrophobic surface. It can be seen that this surface exhibits strong signals of O 1s, Si 2p, and F 1s and a weak signal of C 1s. Fig. 2f gives the XPS high-resolution of C 1s. After modification with THFS, the C1s spectra could be fitted to five peaks at binding energies of 285.3, 286.2, 289.8, 292.3, and 294.8 eV, corresponding to C-C, C-O, CF$_2$-CH$_2$, CF$_2$-CF$_2$ and CF$_3$-CH$_2$, respectively [29]. These results proved the presence of low surface energy groups on the modified SiO$_2$ surfaces, which bring superhydrophobicity to the coating.
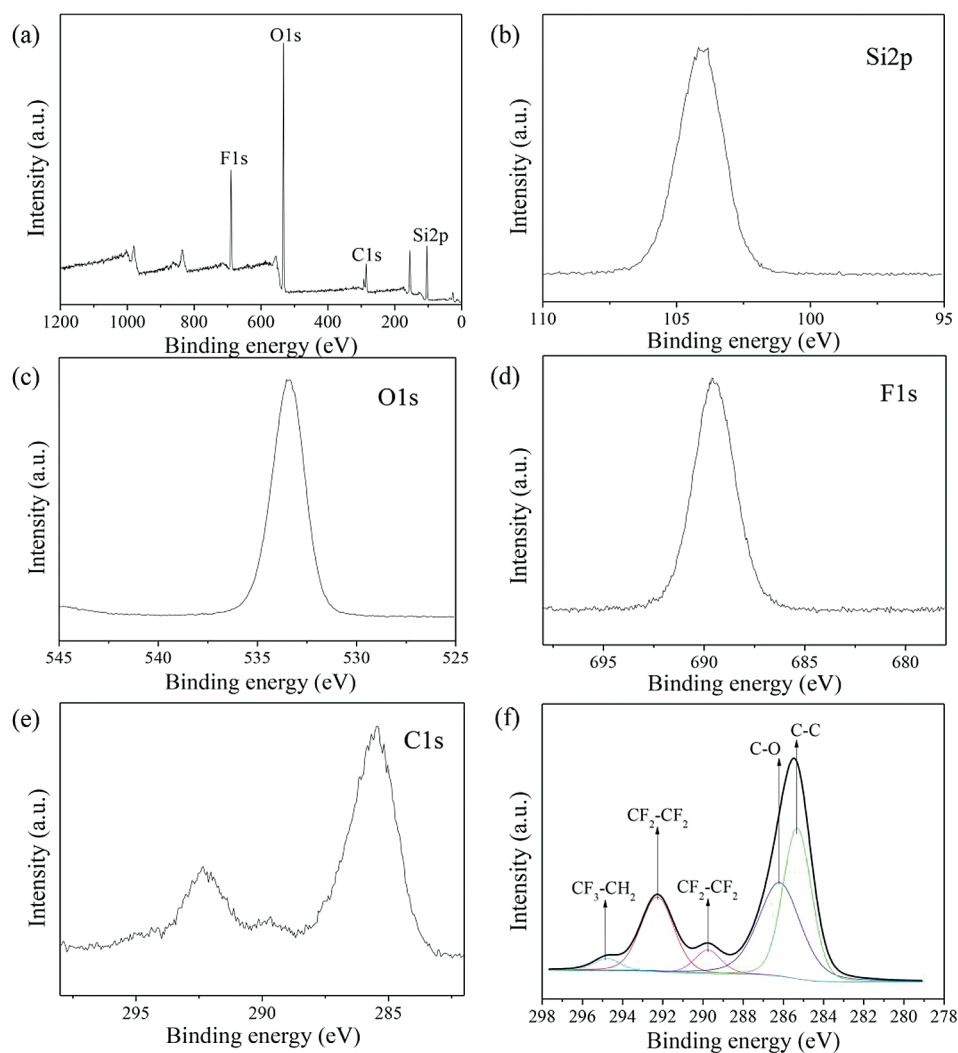

Figure 2: XPS spectra of the superhydrophobic surface: (a) XPS survey spectra, (b) Si 2p, (c) O 1s, (d) F 1s, (e) C 1s, and (f) high-resolution of C 1s

Fig. 3 depicts the test result of the superhydrophobicity of the sample. As shown in Fig. 3a, the droplets on the superhydrophobic coating appear spherical in shape, with a WCA of 152.9° and a SA of 2.7°. The TPU/SH-SiO$_2$ coating also displays strong repellency to the glycerol (Fig. 3e). The coating with superoleophobicity can avoid being wetted by oil and contribute to maintaining long-term superhydrophobicity [30]. We configured different concentrations of sulfuric acid and sodium hydroxide solution to simulate different pH environments (Fig. 3g). When the pH is at the range of 1–11, the CAs are kept at about 153.0° and the SAs are less than 10.0°. As the pH increases from 11 to 13, however, the CAs decrease from 151.7° to 130.4°. This result may explain by the chemical reaction between strong alkaline droplets and the floating SH-SiO$_2$ nanoparticles, which destroys the structure of the coatings [31]. The TPU/SH-SiO$_2$ superhydrophobic coating was studied further for its self-cleaning performance and anti-wetting behaviour. From Fig. 3h, the quartz sand particles on the superhydrophobic surface are carried away by falling water drops, showing excellent self-cleaning properties. In the water jetting test, the water flow is constantly rebounded and cannot wet the superhydrophobic surface due to the low surface energy and the special microstructure which can lock the air inside (Fig. 3i). As shown in Fig. 3j, when the superhydrophobic coating is immersed in water, the air in the microstructure forms a mirror-like film separating the water from the sample.
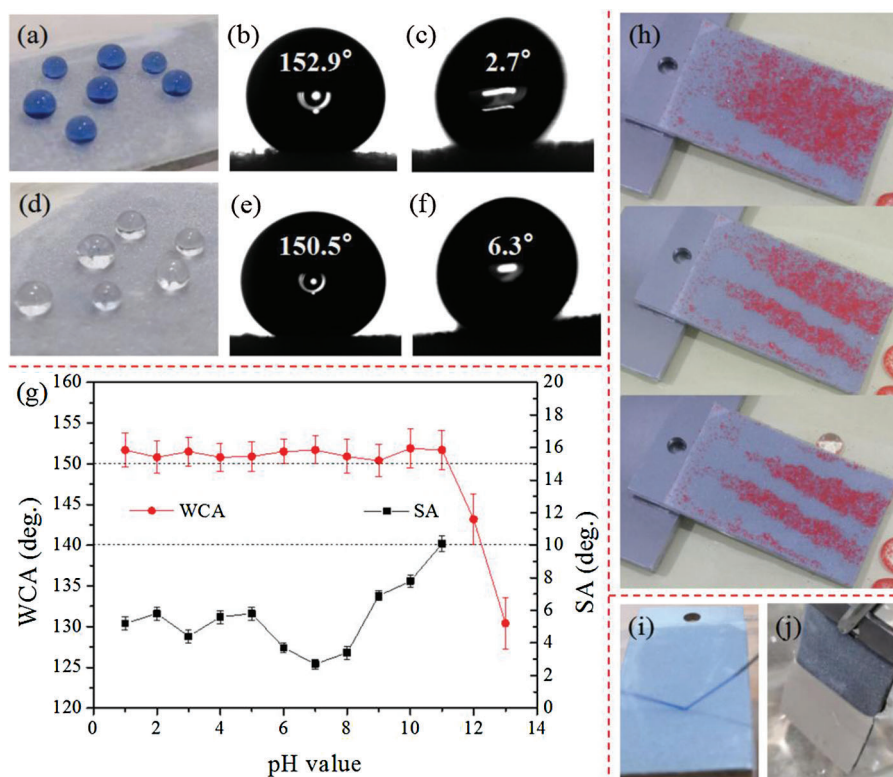

Figure 3: The wettability of the TPU/SH-SiO$_2$ coatings. Photos of spherical (a) water and (d) glycerol droplets on the superhydrophobic surface, and the corresponding (b) (e) WCAs and (c) (f) SAs; (g) CAs and SAs at different pH values (adjusted by H$_2$SO$_4$ or NaOH addition); (h) self-cleaning performance; (i) water jetting test; (j) immersion test

3.2 Anti-Abrasion Test

The weakness of microstructure and the fragility of low-surface-energy materials are two primary obstacles to prevent superhydrophobic coatings from practical engineering applications. In this work, the

resistance of the TPU/SH-SiO$_2$ coating against sand abrasion was illustrated in Fig. S2 in Section 2 of Supplementary Information. The water wettability after each cycle of tests was investigated and is summarized in Figs. 4a and 4b. During the abrasion test, the WCAs of the three different loads remain above 140°, but the decreasing SAs indicate that the low adhesion of the surface was gradually weakened. SEM images of worn surfaces can explain this result. Figs. 4c and 4d reveal little change of the surface morphology, with the micro-nano structure largely retained after 24 abrasion cycles under 2.5 kPa pressure. When the pressure increased to 5 kPa and even 10.0 kPa, obvious mechanical abrasion indentations appeared on the sample surface (marked by red lines in Figs. 4e and 4f). Corresponding surface profiles and roughness data are shown in Fig. S3. The microstructure, which was not completely destroyed, maintains a certain roughness and a high WCA of water on the coating surfaces. However, the weakened microstructure changes the wetting morphology of water droplets, that is, from Cassie-Baxter state to a partially wetting state, which increases the adhesion of water [32].
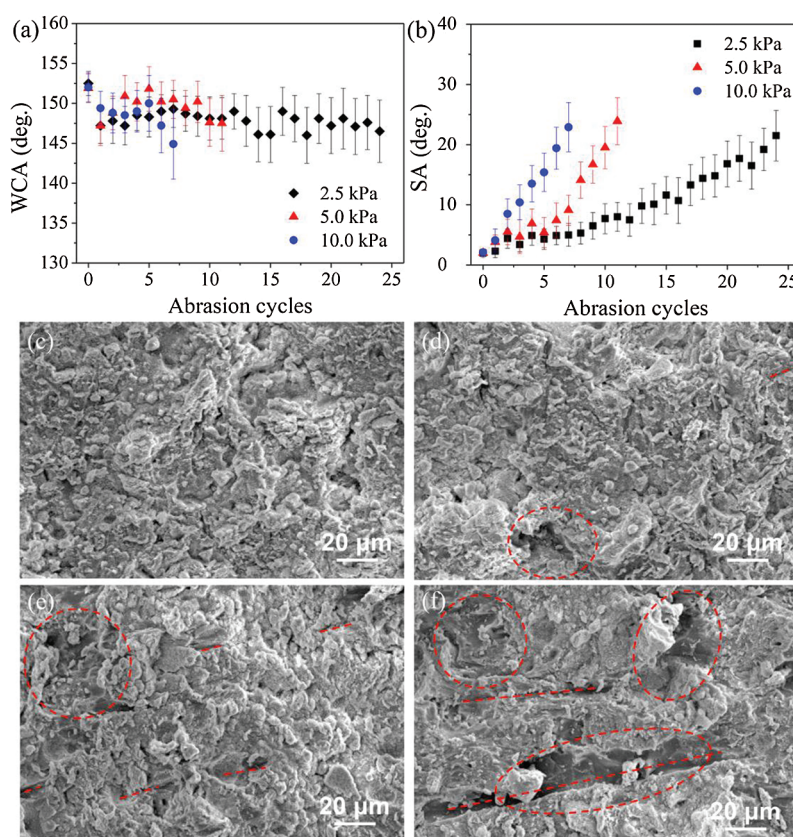

Figure 4: The change of (a) WCAs and (b) SAs of the sample surfaces with abrasion cycles under three different loads; SEM images of (c) as-prepared TPU/SH-SiO$_2$ film and the polished surfaces (d) 2.5 kPa after 24 abrasion cycles, (e) 5.0 kPa after 12 cycles and (f) 10.0 kPa after 7 cycles

The WCAs and SAs of the samples are 146.5° and 21.5° after 24 abrasion cycles under 2.5 kPa pressure, 147.5° and 23.9° after 12 cycles under 5.0 kPa and 144.9° and 22.9° after 7 cycles under 10.0 kPa, respectively. It should be noted that the anti-abrasion ability obtained in this research is much better than previous reports [33–36]. The excellent abrasion resistance of the TPU/SH-SiO$_2$ coating can be explained from three aspects: the characteristics of raw materials, the preparation strategy and the special structure.

Firstly, the robustness of the coating comes from the multi-hydrophobization strategy, which maintains the superhydrophobicity through a layer-by-layer SH-SiO$_2$ removal when subjected to mechanical wear [37,38]. Secondly, the high hardness SH-SiO$_2$ in the top can enhance the mechanical strength of the coating, while the TPU layer in the bottom as a high elastic substrate can reduce the stress at the sharp contact point [39,40]. Finally, the TPU layer can provide physical support for the partially embedded nanoparticles and protect them from being abraded when the floating SH-SiO$_2$ were removed [25,28].

In the following tests, we chose the samples polished at 5.0 kPa for 12 cycles to test with the complete film and bare metal to evaluate the comprehensive performance of the TPU/SH-SiO$_2$ coating.

3.3 Icephobic Characteristics

In this section, icing-delay time is used to evaluate the anti-icing property of the TPU/SH-SiO$_2$ coating. During the freezing process, the droplets will not freeze immediately when they contact the cold surface. After a period of the liquid state, the droplets become turbid with the growth of ice. The stage before becoming turbid is defined as the precooling period, and the following stage is the ice growth period [41], as marked in Fig. 5. On the uncoated Q235 substrate, the water droplet completely freezes at a very fast speed after contacting the supercooled surface, and the whole process takes only 1.056 s. In contrast, the superhydrophobic surface extends the pre-cooling time by more than 200 times, and the entire icing process takes 100 s. TPU/SH-SiO$_2$ coating greatly delays the water freezing process of the supercooled surface, which could be explained by the Cassie-Baxter wetting theory. The air trapped by the micro-nano structure and the extremely small solid-liquid contact area make it difficult for the droplets to transfer heat to the cold surface (Fig. 5b), thereby achieving the purpose of prolonging icing. The surface after abrasion displays slightly decreases pre-cooling time and total icing time compared with the as-prepared surface. Nevertheless, it performs much better than the uncoated substrate.
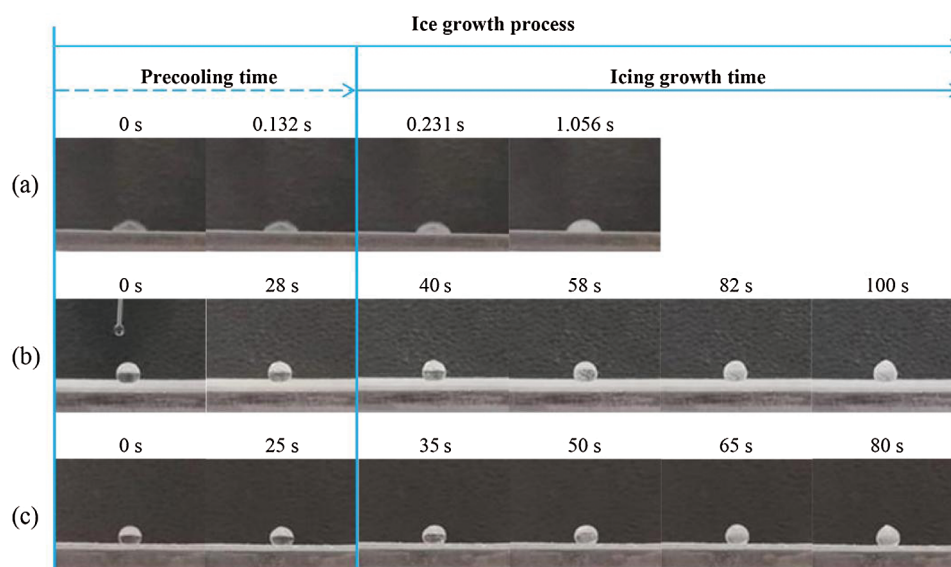

Figure 5: Freezing processes of water droplets (20 µL) on different samples at −20°C: (a) The bare Q235; (b) the complete TPU/SH-SiO$_2$ coating; (c) the polished TPU/SH-SiO$_2$ coating

Furthermore, the droplet impact behaviour was also used to evaluate the dynamic superhydrophobic performance of the coating at −20°C (Fig. 6). In the low-temperature environment, the droplet could not rebound when the cooling droplet hit the uncoated surface (Fig. 6a). On the contrary, the droplet could be

completely rebounded by superhydrophobic coating (Fig. 6b), verifying its advantageous icephobic ability. Even if the water droplet touches the polished surface, similar rebounding is observed, although the time for complete bouncing off the surface is longer (Fig. 6c). These results, together with the ice accumulation results (Section 3 of Supplementary Information), confirm the anti-icing characteristics of the TPU/SH-SiO$_2$ coating even after part of the surface was removed by sandpaper polishing.

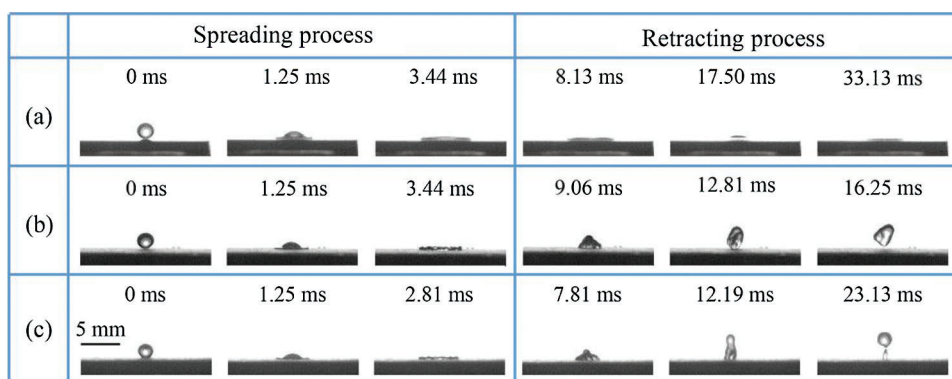|	Spreading process			Retracting process		
	0 ms	1.25 ms	3.44 ms	8.13 ms	17.50 ms	33.13 ms
(a)						
	0 ms	1.25 ms	3.44 ms	9.06 ms	12.81 ms	16.25 ms
(b)						
	0 ms	1.25 ms	2.81 ms	7.81 ms	12.19 ms	23.13 ms
(c) 5 mm						

Figure 6: The moving process of impact droplets (20 μL) on the three sample surfaces with the impact height of 10 cm: (a) The bare Q235; (b) the complete TPU/SH-SiO$_2$ coating; (c) the polished TPU/SH-SiO$_2$ coating. Each sample was frozen at −20°C for 3 h before the test, and cooling droplets were fell from the height of 10 cm. (a) The bare Q235, (b) the TPU/SH-SiO$_2$ coating, (c) the coating after sandpaper polishing

3.4 Corrosion Resistance

To evaluate the corrosion resistance of the TPU/SH-SiO$_2$ coating in corrosive environment, samples were put into the 3.5 wt% NaCl aqueous solution. The electrochemical test results are shown in Fig. 7. The anti-corrosion performance of the coatings in other two corrosive media was also investigated, and the results are discussed in Section 4 of Supplementary Information.

The potentiodynamic polarization curves of bare Q235, TPU/SH-SiO$_2$ coating, and the polished TPU/SH-SiO$_2$ coating in NaCl aqueous were obtained by the Tafel extrapolation method and displayed in Fig. 7a. The corrosion current density (I_{corr}) and corrosion potential (E_{corr}) are summarized in Table S1. It can be seen that when the surface became superhydrophobic, the I_{corr} of the TPU/SH-SiO$_2$ coating is reduced by nearly 1500 times, and the E_{corr} is also significantly shifted from −0.676 V to −0.124 V. A lower I_{corr} and higher E_{corr} mean that the samples have better corrosion resistance due to the superhydrophobic coating [42]. As expected, the TPU/SH-SiO$_2$ coating could withstand the sandpaper polishing and still display good corrosion resistance. The I_{corr} of the polished sample is still far lower than that of bare Q235 steel. Although mechanical wear increases the corrosion rate and I_{corr} of the coated samples, the relevant values are still much lower than those of the bare sample (The relevant data is listed in Table S1 in Section 4 of Supplementary Information).

The EIS results of different samples, including Nyquist plot, and Bode plots, are shown in Figs. 7b–7d. In order to accurately analyze the impedance data, the equivalent circuit model shown in Fig. 7d was used to fit the EIS results and the derived parameters were summarized in Table S2. Three samples show the typical behavior of a system with one time constant (Fig. 7d), which means the systems could be modeled by a sample circuit made of a unique RC-like parallel connection [1,43]. Here, R_s is the solution resistance. R_c and Q_c represent the charge transfer resistance and the constant phase element (CPE), respectively.
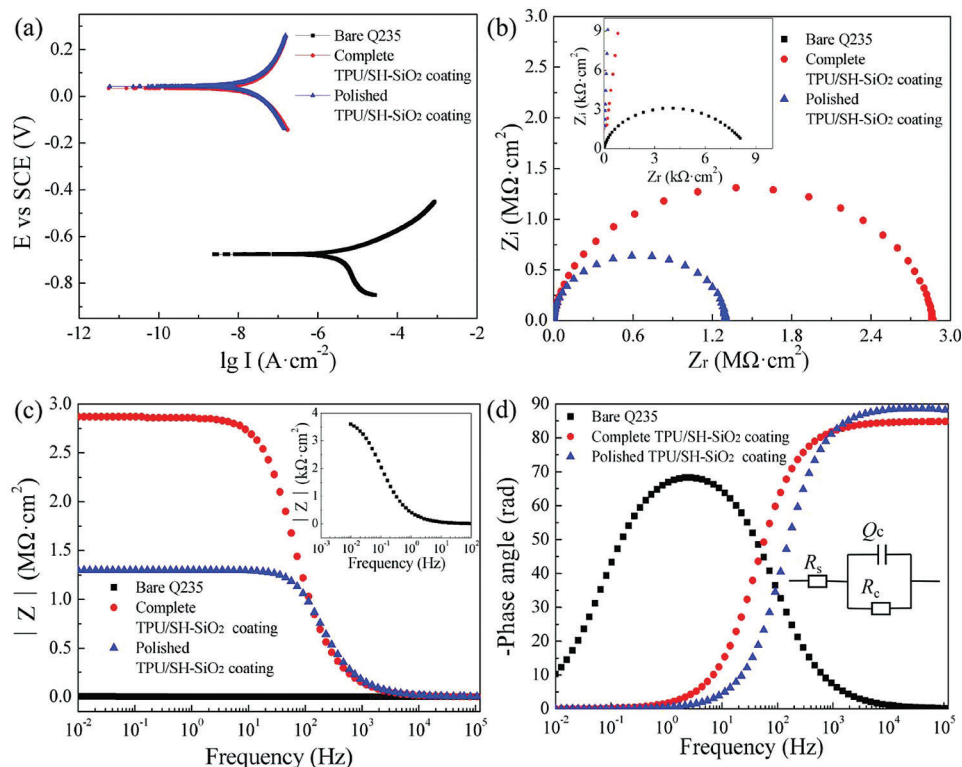
Figure 7: (a) Potentiodynamic polarization curves, (b) Nyquist plots, (c) Bode-|Z| *vs.* frequency plots, and (d) Bode-phase angle *vs.* frequency plots of the bare Q235, the complete TPU/SH-SiO$_2$ coating, and the polished TPU/SH-SiO$_2$ coating measured in 3.5 wt% NaCl aqueous solution; the illustration in (d) is the equivalent electrical circuit for these three samples

As shown in Fig. 7b, the EIS diagrams of the three samples show only one capacitive loop, and the difference between them only lies in the loop's size. Larger capacitive loops are observed for the complete and polished coatings compared to the bare Q235 steel, which indicates the excellent barrier performance of the coating. Such a result can also be proved by Bode-|Z| *vs.* frequency plots [44]. In Fig. 7c, the impedance modulus at the lowest measurement frequency ($|Z|_{0.01Hz}$) reaches 2.2 MΩ·cm^2, and the after-abrasion sample displays 0.84 MΩ·cm^2, which are much larger than bare metal. From Fig. 7d, the bare substrate presents one time constant at low frequency (1–10 Hz). For coated substrates, the phase angle is close to 90° high-frequency domain and only one time constant is displayed. Although the sample degenerates from superhydrophobic to hydrophobic after abrasion, the barrier properties of the coating surface play a role in reducing or preventing the corrosive medium particles from reaching the bare substrate. In summary, the prepared TPU/SH-SiO$_2$ coating has a good protective effect on the Q235 metal substrate before and after the abrasion.

4 Conclusions

In summary, we develop an environment-friendly, cost-effective and simple method to manufacture a durable superhydrophobic coating with TPU and SH-SiO$_2$. SH-SiO$_2$ particles are used to form the surface roughness, and TPU is used as the binder between SH-SiO$_2$ and Q235 substrate. This TPU/SH-SiO$_2$ coating could withstand the abrasion by sandpaper for 24 cycles under a load of 2.50 kPa, showing a robust resistance to sandpaper abrasion. This enhancement of the mechanical stability can be attributed to three factors: the characteristics of raw materials, the preparation strategy and the special structure.

The TPU/SH-SiO$_2$ coating exhibits excellent anti-icing performance. The water droplets need to spend the time of ~100 s to freeze completely at −20°C, showing the increased about 100 times of icing-delay performance comparing with the bare substrate. The anti-corrosion resistance of the superhydrophobic coating is estimated by potentiodynamic and EIS measurement in a 3.5 wt% NaCl solution. The results demonstrate that the corrosion resistance of Q235 steel is significantly improved, which benefited from the barrier properties of the TPU/SH-SiO$_2$ coating. We believe that such a superhydrophobic film with excellent mechanical stability can satisfy the urgent needs of anti-corrosion and anti-icing in practical engineering applications, and its adoption will help to conserve natural resources, cut down energy consumption, and reduce environmental pollution.

Conflicts of Interest: The authors declare that they have no conflicts of interest to report regarding the present study.

References

1. He, S. J., Wang, Z., Hu, J., Zhu, J. B., Wei, L. P. et al. (2018). Formation of superhydrophobic micro-nanostructured iron oxide for corrosion protection of N80 steel. *Materials & Design, 160,* 84–94. DOI 10.1016/j.matdes.2018.09.002.

2. Xiang, T. F., Ding, S. B., Li, C., Zheng, S. L., Hu, W. et al. (2017). Effect of current density on wettability and corrosion resistance of superhydrophobic nickel coating deposited on low carbon steel. *Materials & Design, 114(13),* 65–72. DOI 10.1016/j.matdes.2016.10.047.

3. Wang, S. L., Liu, C. Y., Liu, G. C., Zhang, M., Li, J. et al. (2011). Fabrication of superhydrophobic wood surface by a sol-gel process. *Applied Surface Science, 258(2),* 806–810. DOI 10.1016/j.apsusc.2011.08.100.

4. Ogihara, H., Xie, J., Okagaki, J., Saji, T. (2012). Simple method for preparing superhydrophobic paper: Spray-deposited hydrophobic silica nanoparticle coatings exhibit high water-repellency and transparency. *Langmuir, 28(10),* 4605–4608. DOI 10.1021/la204492q.

5. Zhou, H., Wang, H. X., Niu, H. T., Gestos, A., Wang, X. G. et al. (2012). Fluoroalkyl silane modified silicone rubber/nanoparticle composite: A super durable, robust superhydrophobic fabric coating. *Advanced Materials, 24(18),* 2409–2412. DOI 10.1002/adma.201200184.

6. Shen, Y. Z., Wu, Y., Tao, J., Zhu, C. L., Chen, H. F. et al. (2018). Spraying fabrication of durable and transparent coatings for anti-icing application: Dynamic water repellency, icing delay, and ice adhesion. *ACS Applied Materials & Interfaces, 11(3),* 3590–3598. DOI 10.1021/acsami.8b19225.

7. Huang, Y. F., Hu, M. J., Yi, S. P., Liu, X. H., Li, H. B. et al. (2012). Preparation and characterization of silica/fluorinated acrylate copolymers hybrid films and the investigation of their icephobicity. *Thin Solid Films, 520(17),* 5644–5651. DOI 10.1016/j.tsf.2012.04.067.

8. Emelyanenko, A. M., Boinovich, L. B., Bezdomnikov, A. A., Chulkova, E. V., Emelvaneko, K. A. (2017). Reinforced superhydrophobic coating on silicone rubber for longstanding anti-icing performance in severe conditions. *ACS Applied Materials & Interfaces, 9(28),* 24210–24219. DOI 10.1021/acsami.7b05549.

9. Farhadi, S., Farzaneh, M., Kulinich, S. A. (2011). Anti-icing performance of superhydrophobic surfaces. *Applied Surface Science, 257(14),* 6264–6269. DOI 10.1016/j.apsusc.2011.02.057.

10. Yang, J., Li, W. (2013). Preparation of superhydrophobic surfaces on Al substrates and the anti-icing behavior. *Journal of Alloys and Compounds, 576(6),* 215–219. DOI 10.1016/j.jallcom.2013.04.060.

11. Shen, Y. Z., Tao, H. J., Chen, S. L., Zhu, L. M., Wang, T. et al. (2015). Icephobic/anti-icing potential of superhydrophobic Ti$_6$Al$_4$V surfaces with hierarchical textures. *RSC Advances, 5(3),* 1666–1672. DOI 10.1039/C4RA12150C.

12. Barkhudarov, P. M., Shah, P. B., Watkins, E. B., Doshi, D. A., Brinker, C. J. et al. (2008). Corrosion inhibition using superhydrophobic films. *Corrosion Science, 50(3),* 897–902. DOI 10.1016/j.corsci.2007.10.005.

13. Gao, S. W., Dong, X. L., Huang, J. Y., Dong, J. N., Cheng, Y. et al. (2018). Co-solvent induced self-roughness superhydrophobic coatings with self-healing property for versatile oil-water separation. *Applied Surface Science, 459,* 512–519. DOI 10.1016/j.apsusc.2018.08.041.

14. Zheng, S. L., Li, C., Fu, Q. T., Hu, W., Xiang, T. F. et al. (2018). Development of stable superhydrophobic coatings on aluminum surface for corrosion-resistant, self-cleaning, and anti-icing applications. *Materials & Design, 93,* 261–270. DOI 10.1016/j.matdes.2015.12.155.

15. Wang, N., Xiong, D. S., Deng, Y. L., Shi, Y., Wang, K. (2015). Mechanically robust superhydrophobic steel surface with anti-icing, UV-durability, and corrosion resistance properties. *ACS Applied Materials & Interfaces, 7(11),* 6260–6272. DOI 10.1021/acsami.5b00558.

16. Ma, L. W., Wang, J. K., Zhang, Z. J., Kang, Y., Sun, M. X. et al. (2021). Preparation of a superhydrophobic TiN/PTFE composite film toward self-cleaning and corrosion protection applications. *Journal of Materials Science, 56(2),* 1413–1425. DOI 10.1007/s10853-020-05364-1.

17. Lu, Y., Xu, W. J., Song, J. L., Lin, X., Xing, Y. J. et al. (2012). Preparation of superhydrophobic titanium surfaces via electrochemical etching and fluorosilane modification. *Applied Surface Science, 263,* 297–301. DOI 10.1016/j.apsusc.2012.09.047.

18. Yin, L., Zhang, H. F., Li, Y. Y., Wang, Y., Zhang, R. M. et al. (2016). Fabrication of biomimetic superhydrophobic steel surface under an oxygen rich environment. *Applied Surface Science, 380,* 40–46. DOI 10.1016/j.apsusc.2016.02.090.

19. Ivanova, E. P., Truong, V. K., Wang, J. Y., Berndt, C. C., Jones, R. T. et al. (2010). Impact of nanoscale roughness of titanium thin film surfaces on bacterial retention. *Langmuir, 26(3),* 1973–1982. DOI 10.1021/la902623c.

20. Dar, M. A., Kim, Y. S., Kim, W. B., Sohn, J. M., Shin, H. S. (2008). Structural and magnetic properties of CuO nanoneedles synthesized by hydrothermal method. *Applied Surface Science, 254(22),* 7477–7481. DOI 10.1016/j.apsusc.2008.06.004.

21. Wu, B., Zhou, M., Li, J., Ye, X., Li, G. et al. (2009). Superhydrophobic surfaces fabricated by microstructuring of stainless steel using a femtosecond laser. *Applied Surface Science, 256(1),* 61–66. DOI 10.1016/j.apsusc.2009.07.061.

22. Sethi, S., Dhinojwala, A. (2009). Superhydrophobic conductive carbon nanotube coatings for steel. *Langmuir, 25(8),* 4311–4313. DOI 10.1021/la9001187.

23. Milionis, A., Loth, E., Bayer, I. S. (2016). Recent advances in the mechanical durability of superhydrophobic materials. *Advances in Colloid and Interface Science, 229,* 57–79. DOI 10.1016/j.cis.2015.12.007.

24. Verho, T., Bower, C., Andrew, P., Franssila, S., Ikkala, O. et al. (2011). Mechanically durable superhydrophobic surfaces. *Advanced Materials, 23(5),* 673–678. DOI 10.1002/adma.201003129.

25. Wang, P., Wei, W. D., Li, Z. Q., Duan, W., Han, H. L. et al. (2020). A superhydrophobic fluorinated PDMS composite as a wearable strain sensor with excellent mechanical robustness and liquid impalement resistance. *Journal of Materials Chemistry A, 8(6),* 3509–3516. DOI 10.1039/C9TA13281C.

26. Wang, X. L., Liu, X. J., Zhou, F., Liu, W. M. (2011). Self-healing superamphiphobicity. *Chemical Communications, 47(8),* 2324–2326. DOI 10.1039/C0CC04066E.

27. Groten, J., Rühe, J. (2013). Surfaces with combined microscale and nanoscale structures: A route to mechanically stable superhydrophobic surfaces? *Langmuir, 29(11),* 3765–3772. DOI 10.1021/la304641q.

28. Wang, P., Chen, M. J., Han, H. L., Fan, X. L., Liu, Q. (2016). Transparent and abrasion-resistant superhydrophobic coating with robust self-cleaning function in either air or oil. *Journal of Materials Chemistry A, 4,* 7869–7874. DOI 10.1039/C6TA01082B.

29. Saengkaew, J., Le, D., Samart, C., Sawada, H., Nishida, M. et al. (2018). Superhydrophobic coating from fluoroalkylsilane modified natural rubber encapsulated SiO_2 composites for self-driven oil/water separation. *Applied Surface Science, 462,* 164–174. DOI 10.1016/j.apsusc.2018.08.059.

30. Deng, X., Mammen, L., Butt, H. J., Vollmer, D. (2012). Candle soot as a template for a transparent robust superamphiphobic coating. *Science, 335(6064),* 67–70. DOI 10.1126/science.1207115.

31. Li, S. Q., Liu, X. W., Li, L., Zhang, H. F., Qiu, C. J. (2019). Drag-reductive and anti-corrosive superhydrophobic surface fabricated on aluminum with thin PDMS/SiO$_2$ coating. *Materials Research Express, 6(10)*. DOI 10.1088/2053-1591/ab3c90.

32. Feng, X. J., Jiang, L. (2006). Design and creation of superwetting/antiwetting surfaces. *Advanced Materials, 18(23),* 3063–3078. DOI 10.1002/adma.200501961.

33. Wang, Z., Zhu, H. B., Cao, N., Du, R. K., Liu, Y. Q. et al. (2017). Superhydrophobic surfaces with excellent abrasion resistance based on benzoxazine/mesoporous SiO$_2$. *Materials Letters, 186,* 274–278. DOI 10.1016/j.matlet.2016.10.010.

34. Zhang, Y. F., Ge, D. T., Yang, S. (2014). Spray-coating of superhydrophobic aluminum alloys with enhanced mechanical robustness. *Journal of Colloid and Interface Science, 423,* 101–107. DOI 10.1016/j.jcis.2014.02.024.

35. Su, F. H., Yao, K. (2014). Facile fabrication of superhydrophobic surface with excellent mechanical abrasion and corrosion resistance on copper substrate by a novel method. *ACS applied Materials & Interfaces, 6(11),* 8762–8770. DOI 10.1021/am501539b.

36. Song, J. L., Zhao, D. Y., Han, Z. J., Xu, W., Lu, Y. et al. (2017). Super-robust superhydrophobic concrete. *Journal of Materials Chemistry A, 5(28),* 14542–14550. DOI 10.1039/C7TA03526H.

37. Peng, C. Y., Chen, Z. Y., Tiwari, M. K. (2018). All-organic superhydrophobic coatings with mechanochemical robustness and liquid impalement resistance. *Nature Materials, 17(4),* 355–360. DOI 10.1038/s41563-018-0044-2.

38. Zhang, F., Xu, D., Zhang, D. W., Ma, W. L., Wang, J. K. et al. (2021). A durable and photothermal superhydrophobic coating with entwinned CNTs-SiO$_2$ hybrids for anti-icing applications. *Chemical Engineering Journal, 423(12),* 130238. DOI 10.1016/j.cej.2021.130238.

39. Liu, F., Wang, S. L., Zhang, M., Ma, M. L., Wang, C. Y. et al. (2013). Improvement of mechanical robustness of the superhydrophobic wood surface by coating PVA/SiO$_2$ composite polymer. *Applied Surface Science, 280,* 686–692. DOI 10.1016/j.apsusc.2013.05.043.

40. Li, Y. S., Shao, H., Lv, P. F., Tang, C. Y., He, Z. K. et al. (2018). Fast preparation of mechanically stable superhydrophobic surface by UV cross-linking of coating onto oxygen-inhibited layer of substrate. *Chemical Engineering Journal, 338,* 440–449. DOI 10.1016/j.cej.2018.01.044.

41. Shen, Y. Z., Xie, X. Y., Xie, Y. H., Tao, J., Jiang, J. W. et al. (2019). Statistically understanding the roles of nanostructure features in interfacial ice nucleation for enhancing icing delay performance. *Physical Chemistry Chemical Physics, 21(36),* 19785–19794. DOI 10.1039/C9CP04103F.

42. Cheng, Y. Y., Lu, S. X., Xu, W. G., Wen, H. D. (2015). Fabrication of Au-AlAu$_4$-Al$_2$O$_3$ superhydrophobic surface and its corrosion resistance. *RSC Advances, 5(20),* 15387–15394. DOI 10.1039/C4RA12909A.

43. Koochaki, M. S., Khorasani, S. N., Neisiany, R. E., Ashrafi, A., Trasatti, S. P. et al. (2021). A highly responsive healing agent for the autonomous repair of anti-corrosion coatings on wet surfaces. In operando assessment of the self-healing process. *Journal of Materials Science, 56(2),* 1794–1813. DOI 10.1007/s10853-020-05332-9.

44. Hinderliter, B. R., Croll, S. G., Tallman, D. E., Su, Q., Bierwagen, G. P. (2006). Interpretation of EIS data from accelerated exposure of coated metals based on modeling of coating physical properties. *Electrochimica Acta, 51(21),* 4505–4515. DOI 10.1016/j.electacta.2005.12.047.

Supplementary Information

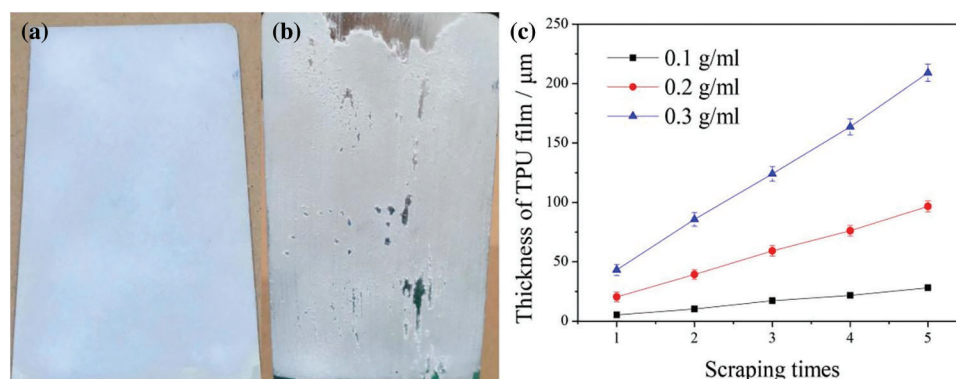## 1 Determination of TPU layer thickness

Figure S1: Optical photos of TPU/SH-SiO$_2$ coating with a thin TPU layer (75 μm) (a) before and (b) after polishing; (c) effect of TPU/DMF film-forming solution concentration and the number of scraping times on the thickness of TPU layer

TPU layer has a great influence on the wear resistance of the TPU/SH-SiO$_2$ coating. Herein, we have prepared superhydrophobic coatings with different thicknesses using TPU/DMF film-forming solution of various concentrations, and polished these surfaces with 80 Grit SiC sandpaper. After testing, it is found that when the thickness of TPU layer is thin, the coating is easy to wear through and expose the metal substrate after polishing (Fig. S1). Therefore, we control the thickness of TPU layer between 150~200 μm using 0.3 g/ml film-forming solution to prepare the coatings in the current work. This can ensure the mechanical properties of the coating and achieve good adhesion between the coating and the metal substrate.
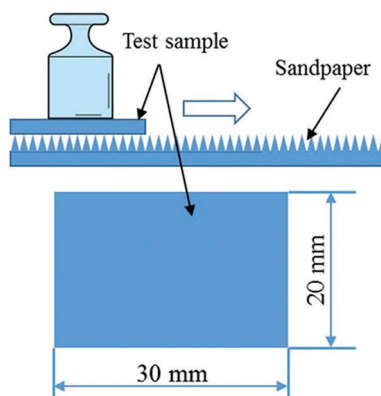
2 Abrasion test

Figure S2: Evaluation of abrasion resistance of coating
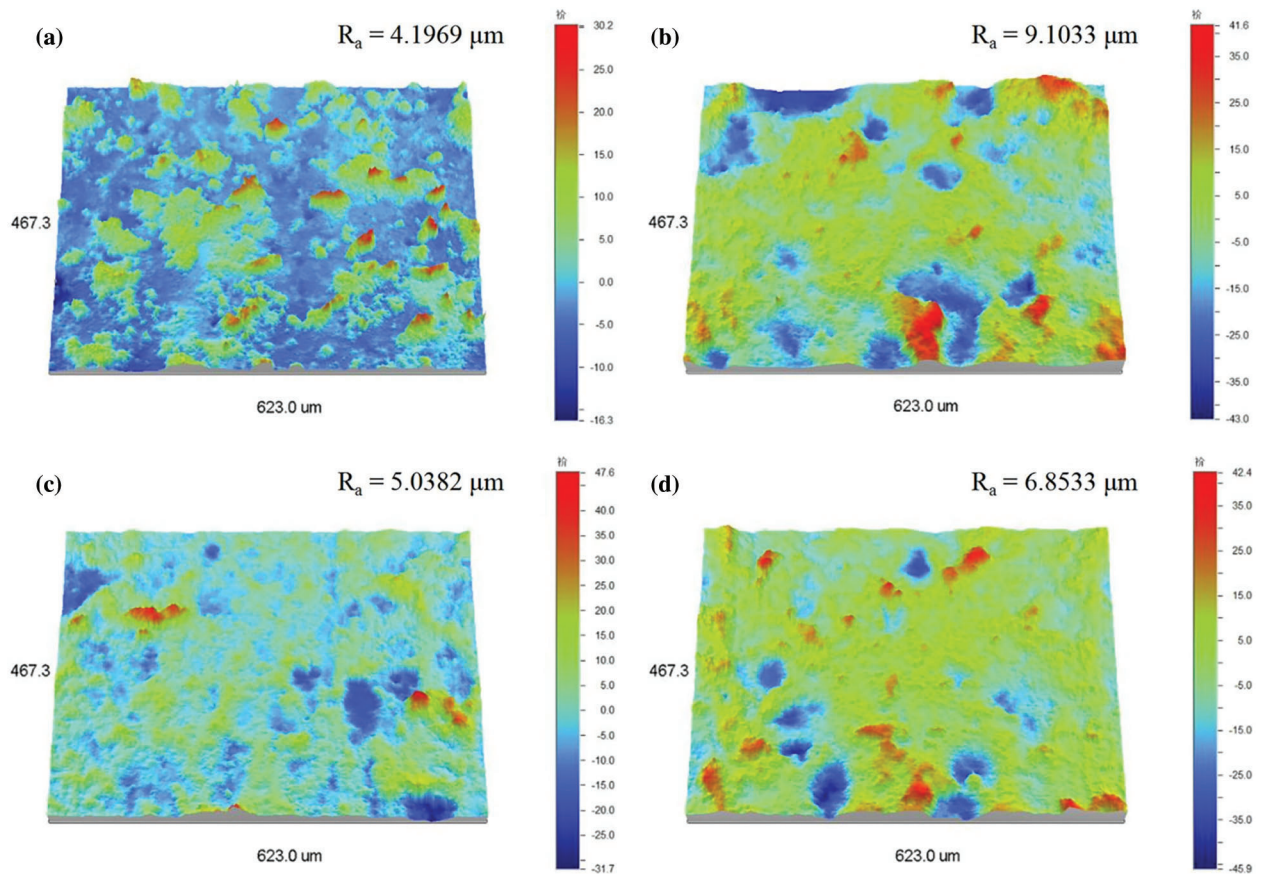
Figure S3: 3D view of surface profiles (300 × 300 μm) and the corresponding roughness data. (a) as-prepared TPU/SH-SiO₂ film and the polished surfaces (b) 2.5 kPa after 24 abrasion cycles, (c) 5.0 kPa after 12 cycles and (d) 10.0 kPa after 7 cycles

3 Accumulation behavior of ice on inclined surface

The optical images of ice accumulation in the experiment also proves the anti-icing performance of superhydrophobic coating (Fig. S4). In this test, 4 ml of ice water was dropped on the samples placed with 10° inclination, and these samples was frozen at −20°C for 3 h in advance. When the droplets touched the smooth and cold surface, they began to freeze and accumulate gradually. At the end of the test, almost all the water stayed on the bare sample and became ice. On the contrary, most of the water droplets rolled off on the as-prepared and the sand-polished samples; only a small portion left and formed ice.
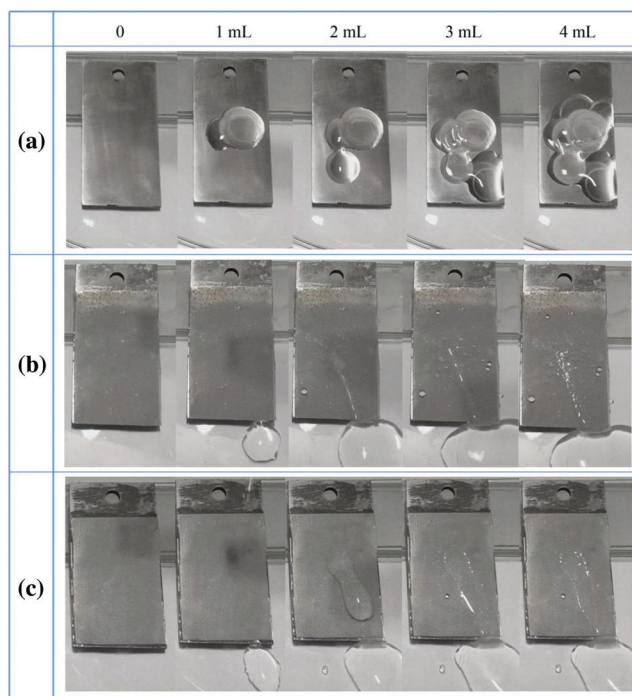
Figure S4: Optical images taken during the ice accumulating on inclined surfaces: (a) The bare Q235; (b) the complete TPU/SH-SiO$_2$ coating; (c) the polished TPU/SH-SiO$_2$ coating. Each substrate was frozen at –20°C for 3 h before the test and placed with 10° inclination

4 Anti-corrosion performance in different corrosion environments

The TPU/SH-SiO$_2$ superhydrophobic coating performed well in strong acid and alkali environments. Compared with the test in 3.5 wt% NaCl aqueous, the coating has improved the corrosion resistance of the metal substrate more obviously. The potentiodynamic polarization curves and Nyquist plots are manifested in Fig. S5, and I_{corr} and E_{corr} displayed in Table S3. The more positive E_{corr}, lower I_{corr}, and much higher impedance of the superhydrophobic coating prove that the metal substrate is effectively protected.

Table S1: Corrosion density (I_{corr}) and Corrosion potential (E_{corr}) of different samples in 3.5 wt% NaCl solution

Specimen	I_{corr} (A·cm^{-2})	E_{corr} (V)	β_a (mv·dec^{-1})	β_c (mv·dec^{-1})	Corrosion Rate (mm/a)
Bare Q235	6.01×10^{-6}	−0.676	84.479	−723.63	6.01×10^{-6}
Complete TPU/SH-SIO$_2$ Coating	1.65×10^{-8}	−0.035	134.85	−129.98	1.65×10^{-8}
Polished TPU/SH-SIO$_2$ coating	1.38×10^{-8}	−0.042	129.98	−115.79	1.38×10^{-8}

Table S2: Impedance parameters of specimens obtained from EIS Equivalent electrical circuit

Specimen	R_S ($\Omega \cdot CM^2$)	Q_C ($\mu F \cdot Cm^{-2}$) (n)	R_C ($\Omega \cdot Cm^2$)
Bare Q235	10.84	5.037×10^{-4} (0.8228)	3849
Complete TPU/SH-SiO$_2$ Coating	0.0041	1.78×10^{-9} (0.9429)	2.89×10^6
Polished TPU/SH-SiO$_2$ Coating	27.4	9.856×10^{-10} (0.9909)	1.30×10^6

Table S3: Corrosion density (I_{corr}) and Corrosion potential (E_{corr}) of diverse samples in other corrosive solutions

Samples	pH = 1 H$_2$SO$_4$ aqueous		PH = 13 NaOH aqueous	
	I_{corr} (A·cm^{-2})	E_{corr} (V)	I_{corr} (A·cm^{-2})	E_{corr} (V)
Bare Q235	4.89×10^{-5}	−0.4350	1.21×10^{-5}	−0.3360
Complete TPU/SH-SiO$_2$ Coating	1.47×10^{-8}	−0.0782	1.40×10^{-8}	−0.0731
Polished TPU/SH-SiO$_2$ Coating	1.37×10^{-7}	−0.0242	1.50×10^{-8}	−0.1476
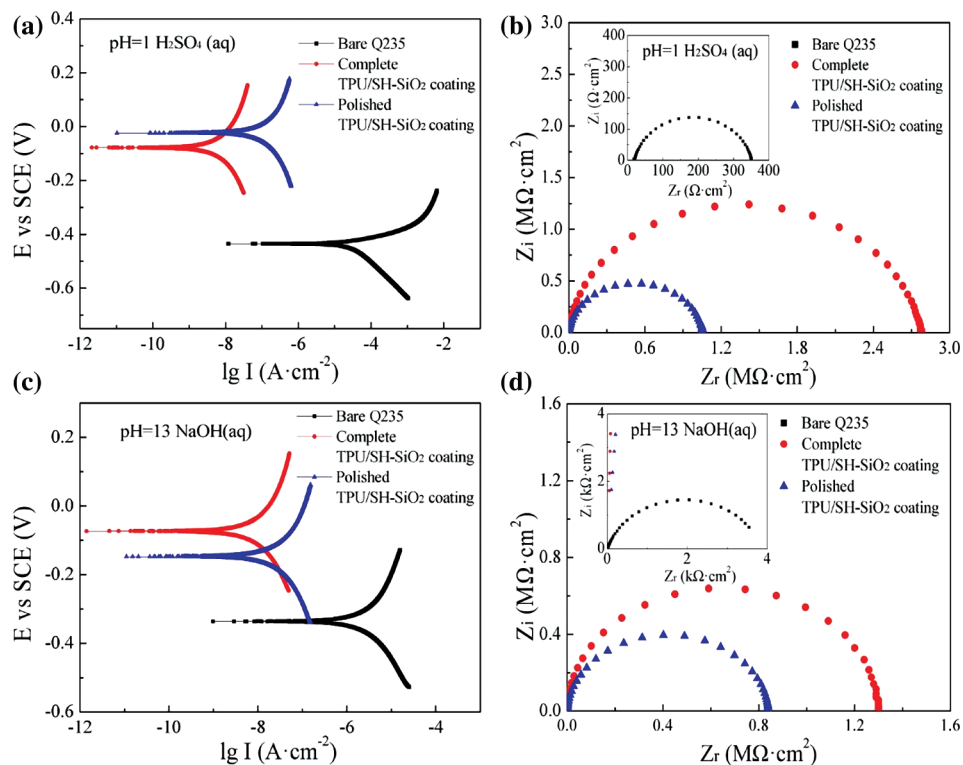
Figure S5: Potentiodynamic polarization and Nyquist plots of diverse samples in different corrosive solutions: (a) (b) pH = 1 H$_2$SO$_4$ aqueous; (c) (d) pH = 13 NaOH aqueous